Energy Reports 12 (2024) 210–225

Contents lists available at ScienceDirect

Energy Reports

journal homepage: www.elsevier.com/locate/egyr

Research paper

Performance prediction of a pump as a turbine using energy loss analysis

Dessie Tarekegn Bantelay [a,*], Girma Gebresenbet [a,b], Bimrew Tamrat Admasu [a], Muluken Temesgen Tigabu [a], Muluken Zegeye Getie [a]

[a] Faculty of Mechanical and Industrial Engineering, Bahir Dar Institute of Technology, Bahir Dar University, 26, Ethiopia
[b] Department of Energy and Technology, Swedish University of Agric Sciences, SLU, Box 7032, Uppsala 750 07, Sweden

ARTICLE INFO

Keywords:
Pump as a turbine
Performance prediction
Energy loss analysis
Numerical study
Analytical method

ABSTRACT

As interest in renewable energy sources grows, interest in small-scale hydropower development and utilization increases. The development of micro- and small-scale hydropower plants is challenging, mainly due to the high cost of hydraulic turbines. If the turbine mode performance can be predicted accurately before installation, pumps as turbines (PATs) are an excellent alternative for small-scale hydropower generation. In this study, a theoretical procedure using a detailed energy loss analysis to determine PAT's energy losses is developed, and a non-dimensional performance prediction model is presented. The models were implemented to determine the pressure, head, torque, power, and efficiency across a wide range of flow rates. This work clearly characterizes the effects of individual losses, thereby acknowledging their influence. The prediction results were tested at ten different flow rates, ranging from 50 % to 180 %. The model result was validated through experiments using a hydro-pump test rig developed at the Bahir Dar Institute of Technology at Bahir Dar University. The numerical and model results have good agreement with the experimental results. at BEP The experimental result gives a 1.6 flow rate, 1.72 head ratios, and an efficiency of 76.53 %, 78.09 %, and 74.04 % using analytical, numerical, and experimental methods, respectively. The PAT off-design efficiency decreases sharply below BEP and smoothly above BEP. At BEP, the CFD and analytical results deviated by −2.04 % and 3.08 %, respectively, from the experimental results. Further, the detailed energy loss analysis revealed that the volute frictional (12.1 %), the throat frictional (11.9 %), the inlet pipe frictional (11.2 %), the impeller frictional (9.4 %), and the volute diffusion (8.9 %) losses take the major energy losses sequentially. This provides full insight for applying performance optimization measures.

1. Introduction

Hydropower generation is one of the most mature and widely used renewable energy technologies. Hydropower accounted for 19.2 % of total energy sources in 2017. However, large hydropower stations dominate the sector, causing serious environmental impacts and forcing residents to relocate, thereby creating a complex social issue (Li et al., 2018). The drawbacks of large-scale hydropower projects enable micro-hydropower to be a preferred option for utilizing hydropower potential in rural areas (Binama et al., 2017). However, small-scale turbines are more expensive compared to large-scale turbines due to the high cost of small conventional turbines. This calls for the development of low-cost turbines with increased efficiency to ensure the plant's financial viability. In this regard, using centrifugal pumps as turbines (PAT) is one of the best viable options (Barbarelli et al., 2016; Muttalli et al., 2014). When water flows in the opposite direction from centrifugal pumps, the same pump can serve as a turbine to generate mechanical energy (Thoma and Kittredge, 1931). Mass production and technological maturation enable centrifugal pumps to be inexpensive, readily available, less complicated, and require less maintenance (Popescu et al., 2013). However, unlike conventional turbines, they lack mechanisms to accommodate flow rate and head variation (Giosio et al., 2015). As a result, they're most efficient at a single operating point in the characteristic curve. When using centrifugal pumps for micro-hydro power utilization, the two most difficult challenges are selecting the right pump for the job and improving poor part-load efficiency (Barbarelli et al., 2016; Derakhshan and Nourbakhsh, 2008). The selection of an appropriate type and size of pump to use as a turbine depends on the available head and flow rate at the site. Research results reported that all single and multistage radially or axially centrifugal pumps can be used as turbines in reverse mode (Derakhshan and Nourbakhsh, 2008;

* Corresponding author.
E-mail addresses: dessie.Tarekegn@bdu.edu.et, dessie2000ec@gmail.com (D.T. Bantelay).

https://doi.org/10.1016/j.egyr.2024.06.023
Received 27 April 2024; Received in revised form 21 May 2024; Accepted 10 June 2024
Available online 15 June 2024

Nomenclature

Symbols

σ	Slip factor
τ	Blade blockage
H	Head
t	Blade (van) thickness
Z	Number of blades(vans)
β	Blade (van) angle
D	Diameter
ω	Rotational speed
A	Area
h	Head loss
b	Impeller blade width
Re	Reynolds number
C	loss coefficient
L	Length
ε	Surface roughness factor
Df	Diffusion factor
λ	Coefficient of friction
CD	Coefficient of diffusion [0.8]
s	Blade solidity factor
δ	Deviation angle
N	Rotational speed
ε	Blade thickness coefficient
U	Circumferential velocity
W	Relative velocity
V	Absolute velocity
ν	kinematic viscosity

Subscript

1	Impeller leading edge
2	Impeller trailer edge
3	Volute
4	Throat inlet
5	Throat outlet
b	Blade
df	Diffusion
fr	Friction loss
hy	Hydraulic
La	Impeller
man	Manometric
p	Pump
r	Real
sh	Shock loss
t	Turbine
th	Theoretical
th	Throat
v	Volute
inf	Ideal
av	Average
bl	Blade loading
me	Mechanical
u	Tangential
r	Radial

Superscript

‘	Actual

Orchard and Klos, 2009). Axial flow pumps are appropriate for low-head, high-flow rate ranges, whereas multistage radial flow pumps are suitable for high-head and low-flow rate applications. The pump works as a turbine most efficiently in the head range of 13–75 m (Buse, 1981). Despite their specific head and flow rate design, centrifugal pumps often function across a wide range of flow rates. During these off-design flow rates, the flow pattern deviates from the desired behavior. Flow separation, recirculation, and backflow are possible. These lead to reduced efficiency and reduce the lifespan and reliability of the components.

Even though catastrophic failures are rare (Bantelay, 2019), prolonged operation at off-design points significantly shortens the lifespan of the pump. When selecting a pump for a reverse mode of operation, it is critical to estimate the system's operating range. The decision regarding the PAT range of operating parameters is associated with identifying a safe operating range and a trade-off between efficiency reduction and operational cost increment. This highlights the necessity for accurate performance prediction of PAT at its best efficient point and during off-design operations. The manufacturer's experiential values are the most reliable method of assessment. Unfortunately, most manufacturers are unfamiliar with reverse mode operation and cannot provide PAT performance curves (Motwani et al., 2013). Moreover, a few manufacturers offer PATs that are 30–100 % more expensive than the same machine when offered as a standard pump. The higher price results from the additional cost of developing PAT know-how, testing, and modifying the standard pump for use as a PAT. This will avert the cost advantage of PATs over conventional turbines. Experimental investigations revealed that at the PAT's BEP, flow rate and head increased with efficiency reduction (Raman et al., 2013). As a result, an understanding of the full operational condition of pumps during turbine mode operation has emerged as a critical research question (Chappallaz, 1992).

Many researchers have attempted to develop PAT's performance prediction models using theoretical, numerical, and experimental techniques since Stepanoff's first theoretical study (Stepanoff, 1957). Table 1 displays the models developed by various researchers for predicting head and discharge. In the early stages, performance prediction of PAT focuses on determining PAT using the pump's BEP and specific speed. Shahram conducted some hydraulic analysis without suggesting any forecasting methods based on his findings. Later, Yang et al. (2012a) developed a similar prediction model to that of Sharma. G. Ventrone also proposed a theoretical prediction model (Sharma, 1985). Furthermore, predictions made using these theoretical methods have not been very reliable, and the results show large deviations when compared to the actual results. Different scholars have also carried out CFD analysis and published their studies. However, their findings are not applicable for selecting an appropriate centrifugal pump before installation. The models derived from theoretical and numerical studies exposed an average error of 20 % from the experimental data and more than 40 % at certain specific speeds (Singh et al., 2010). Besides theoretical and numerical studies, different scholars also published their experimental-based prediction methods (Derakhshan et al., 2008; Nautiyal et al., 2011; Williams, 1994). However, most models derived from experimental results are curve-fitting equations based on a limited number of data points. As a result, the equations are not generic to all shelf pumps and are limited to certain ranges of specific speeds. Although many efforts have been made to improve the accuracy of the models, the model's accuracy still depends on the amount of experimental data. As a result, these methods remain case-dependent and difficult to use across a broad spectrum (Liu et al., 2019a). In addition, most of the methods developed mainly target predicting best efficient point and associated performance.

Performance prediction using energy loss analysis covers a wide range of operation parameters, including diffuser, volute, impeller, and inlet pipe (Kara Omar et al., 2017). Even though it is a powerful method for full flow rate performance prediction, it didn't get proper attention in

Table 1
Performance prediction methods and trends for pumps working as turbines.

References	Methods	Criteria	Head correction factor (h_t/h_p)	Discharge correction factor (Q_t/Q_p)	Remarks
Stepanoff (Stepanoff, 1957)	Theoretical	*BEP* $N_s \approx 40–60$	$1/\eta_{h,p}$	$1/\sqrt{\eta}_{h,p}$	$\eta_{h,p} = \sqrt{\eta_p}$ $P_p = P_t$; $\eta_p = \eta_t$; $N_{st} = N_s\eta_p$
Childs (Childs, 1962)	Theoretical	*BEP*	$1/\eta_p$	$1/\eta_p$	$P_p = P_t$ & $\eta_p = \eta_t$
Hancock (Hancock, 1963)	Theoretical	*BEP*	$1/\eta_t$	$1/\eta_t$	$\eta_p = \eta_t \pm 2$ %
McClaskey and Lundquist (McClaskey, 1976)	Theoretical	*BEP*	$1/\eta_p$	$1/\eta_p$	$P_p = P_t$ & $\eta_p = \eta_t$
Grover (Grover, 1980)	Theoretical	N_s $Ns \approx 10 – 50$	$2.693 – 0.0229N_{st}$	$2.379 – 0.0264N_{st}$	$N_{st} = N_s{}^*\eta_p$ $\eta_t = \eta_p(0.893 – 0.0466\ N_{st})$
Hergt (Williams, 1994)	Experimental	N_s	$1.3 – 6/(N_{st} - 3)$	$1.3 – 1.6/(N_{st} - 5)$	
Sharma (Sharma, 1985)	Theoretical	*BEP*	$\frac{1}{\eta_p^{1.2}}$	$\frac{1}{\eta_p^{0.8}}$	$P_p = P_t$ & $\eta p = \eta t$ *Applied for* N_s: *50–60*
Schmiedl (Schmiedl, 1988)	Experimental	*BEP*	$-1.4 + \frac{2.5}{\eta_p}$	$-1.5 + \frac{2.4}{\eta_p^2}$	$\eta_t = p(1.158 – 0.265\ N_{st})$, $\eta_{hp} = \sqrt{\eta_p{}^{0.5}\eta_t{}^{0.5}}$
Alatorre-Frenk (Alatorre-Frenk and Thomas, 1990)	Experimental	*BEP*	$\frac{1}{0.85\eta_p{}^5 + 0.385}$	$\frac{0.85\eta_p{}^5 + 0.385}{2\eta_p{}^{9.5} + 0.205}$	$\eta_t = \eta_p - 0.03$
Derakshan and Nourbakhsh (Derakhshan and Nourbakhsh, 2008)	Theoretical	N_s	$0.0233(\frac{N_p Q_p^{0.5}}{(gH_p)^{0.75}}) + 0.6464$	$0.9413(\frac{N_p Q_p^{0.5}}{(gH_p)^{0.75}}) + 0.6045$	@ *BEP*
Nautiyal1 (Nautiyal et al., 2011)	Experimental	N_s	$41.667(\frac{\eta_p - 0.212}{\ln(N_{sp})}) - 5,042$	$30.303(\frac{\eta_{BEP,p} - 0.212}{\ln(N_{sp})}) - 3.424$	
Yang et al. (Yang et al., 2012a)	Theoretical	*BEP*	$\frac{1.2}{\eta_p^{1.1}}$	$\frac{1.2}{\eta_p^{0.55}}$	Like Sharma's method
Jain (Jain et al., 2015)	Experimental	Geometry	$\eta_{BEP} = B_0\left(\frac{D}{D_r}\right)^{n_1}\left(\frac{N}{N_r}\right)^{m_1}\exp\left(n_2\left[\ln\left(\frac{D}{D_r}\right)\right]^2\right) \times \exp\left(m_2\left[\ln\left(\frac{N}{N_r}\right)\right]^2\right)$		The coefficients determined by experiment
Tan and Engeda (Tan and Engeda, 2016)		Ns	$\frac{1}{H_{BEP,P}}\left(\frac{\omega D_0}{N_{st}D_{st}g^{0.75}}\right)^2$	$\frac{\omega D_0^3}{Q_{BEP,P}N_{st}D_{st}^3g^{0.75}}$	
Stefanizzi, M., et al., (Stefanizzi et al., 2017)	Experimental	BEP	-0.000023N3S,T + 0.003206N2S,T - 0.145781NS,T + 3.604636		Based on the literature result $NS_T = 0.9237NS_P - 2.6588$
Fontanella, S., (Fontanella et al., 2020)	Experimental	Ns	$1.4568\left(\frac{N_t}{N_p}\right)^2$	$1.3595\frac{N_t}{N_p}$	$N_{st} = 0.8793\ N_{sp}$

PAT performance prediction. Recently presented a successful performance investigation based on loss analysis in pumps (Yang et al., 2012b). Friction, turbulence, and inefficiencies in the pump component design squander a portion of the added energy in both operating modes. Energy loss analysis is a method that quantifies the energy waste in the pump system. The outcome enables the optimization of the PAT's design and operation. This allows for maximizing efficiency, lifetime cost, and reliability of the system. Some researchers conducted comprehensive loss studies without a prediction model (Alatorre-Frenk and Thomas, 1990). Others investigate hydraulic losses in pumps and turbine modes, and they develop a highly detailed loss prediction model that requires detailed geometry and experimental data (Tan and Engeda, 2016). Some researchers limited their theoretical energy loss analysis to PAT performance at BEP rather than at full flow rates (Derakhshan and Nourbakhsh, 2008). Other researchers also conducted a detailed energy loss analysis by type (Barbarelli et al., 2016; Liu et al., 2019a; Wang et al., 2020). Barbarelli (Barbarelli et al., 2016) utilizes pump geometry from manufacturers to ascertain friction and dynamic losses in every component. This method was applied to six centrifugal pumps at BEP and revealed a relative error of up to 21.4 %. Similarly, Liu (Liu et al., 2019a) conducted an in-depth analysis to predict performance in both pump and turbine modes. The results led to the development of a method that relies on volume flow rate to determine BEP. Forecast accuracy improved compared to Barbarelli's method. However, the proposal did not include a predictive model, aside from the comprehensive loss computation. In addition, due to the complexity of computing hydraulic losses in PAT mode, researchers attempt to estimate them directly in pump mode. This makes the models less accurate (Wang et al., 2020). On the other hand, due to the complicated flow path of PAT, it is challenging to determine energy loss distribution using traditional approaches. Consequently, a few researchers were forced to use the entropy generation theory to conduct PAT energy loss analysis (Ghorani et al., 2020; Li et al., 2017; Xin et al., 2022; Yu et al., 2022; Zhou et al., 2022).

Despite much research, developing an accurate model to predict PAT performance and BEP prediction is still in the infant stage. This work conducted a detailed energy loss analysis across a broad spectrum of flow rates using theoretical and numerical methods. Additionally, an iterative method for determining BEP was developed. A detailed energy loss share by components and types was investigated for the full flow range. the accuracy of the result validated using experiments. This work is unique in that it can predict PAT performance and associated energy loss types using a wide range of operation parameters. Four distinct sections, each focusing on a specific aspect of the investigation, make up the research process. Section 1 describes the study's background. Section 2 outlines the research methodology, including hydraulic loss analysis, performance analysis, performance prediction procedures, and numerical modeling techniques. Section 3 presents the key findings, their implications, and a detailed discussion with interpretations and explanations. Section 4 provides a comprehensive conclusion summarizing the main findings, discussing practical implications, and offering recommendations. Overall, this manuscript aims to contribute to existing knowledge by providing a holistic understanding of detailed energy loss analysis in turbines.

2. Materials and methods

Energy loss analysis starts from the analysis of ideal velocity components and ideal head. The ideal pump model considers an infinite number of infinitely thin blades, where the blade profile perfectly guides

the fluid motion and the flow angle equals the blade angle. However, in the real world, centrifugal pumps have a limited number of blades with a certain thickness. As a result, slips and blockages are unavoidable phenomena. The theoretical head calculation considered slip and blade blockage. However, the theoretical head calculation did not account for the various system losses. After considering various hydraulic, leakage, and mechanical friction losses, the real head determined. In this regard, the energy loss analysis commences with an examination of the velocity triangles at both the inlet and outlet of the impeller's blades. As the flow direction in PATs reverses, the velocity triangle changes, as shown in Fig. 1. Considerations show that the inlet flow angle in a PAT is not the same as the outlet flow angle in pump mode. However, the blade tip flow angle (α_2) is approximately equal to the volute angle (αv). Additionally, in pump mode, the fluid enters in the axial direction. As a result, the tangential inlet absolute velocity ($V_{u1,P}$) is considered zero, whereas it has a significant value in turbine mode due to the slip effect. The difference between the ideal and real absolute velocity tangential components was determined using the Stodola equation (Dixon and Hall, 2013). For PAT, the analysis unchangeably uses conventional pump section numbering. Moreover, the mean radius of the blades determined the fluid absolute velocity components used in this analysis.

2.1. Hydraulic losses analysis

Centrifugal pumps suffer from mechanical, disk friction, leakage, and hydraulic losses. Except for hydraulic losses, all losses have the same value in both flow directions. When the flow direction changes, hydraulic losses change dramatically. Hydraulic losses occur due to turbulent motion, surface irregularities, and constraints within the pump components (Derakhshan and Nourbakhsh, 2008). Quantifying each hydraulic loss in a PAT, however, is a challenging task due to the complex fluid dynamics of the flow path. It frequently necessitates detailed empirical correlations and computational analysis. Several experiential correlations and established analytical models for calculating hydraulic losses in the fluid flow path have been presented. Table 2 presents the detailed operational and geometric parameters of the prototype centrifugal pump. The geometrical data using methods developed by some of the authors was determined (Bantelay et al., 2024). The frictional losses at the inlet, impeller, volute, and throat and

Table 2
Key operational and geometric parameters of the case centrifugal pump.

Nominal Parameters	Symbol	Value	Nominal Parameters	Symbol	Value
Design flow rate [m^3/s]	Q_e	*0.03*	*Throat inlet diameter [mm]*	D_4	*63.5*
Design head [m]	H_e	*25.5*	*Throat outlet diameter [mm]*	D_{th}	*79.5*
Rotational speed [RPM]	N	*1450*	*Impeller hydraulic diameter [mm]*	$D_{hy,La}$	*36*
Motor power [kW]	P_e	*10.7*	*Throat hydraulic diameter [mm]*	$D_{hy,th}$	*79.4*
Specific speed [-]	N_s	*1179*	*Inlet length [mm]-$5D_1$*	L_e	*515.5*
Distance between blades inlet [mm]	a_1	*45.1*	*Impeller blade length [mm]*	L_{La}	*217*
Distance between blades outlet [mm]	a_2	*145.5*	*Volute length [mm]*	L_v	*514.6*
Blade (van) inlet width [mm]	b_1	*34.5*	*Throat length [mm]*	L_{th}	*163.5*
Blade(van)outlet width [mm]	b_2	*20.3*	*Blade(van) thickness [mm]-uniform*	t	*8.9*
Volute inlet width [mm]	b_3	*40.6*	*Number of Blades (vans) [no]*	Z	*6*
Impeller Eye diameter [mm]	D_e	*125.5*	*Volute angle [°]*	α_v	*3.5*
Hub diameter [mm]	$D_{1\,H}$	*32.1*	*Blade inlet angle [°]*	β_{b1}	*28*
Blade inlet diameter [mm]	D_1	*103.1*	*Blade outlet angle [°]*	β_{b2}	*12*
Blade tip diameter [mm]	D_2	*295*	*Throat (cone) angle [°]*	θ_{th}	*5.6*
Volute base diameter [mm]	D_3	*327.2*			

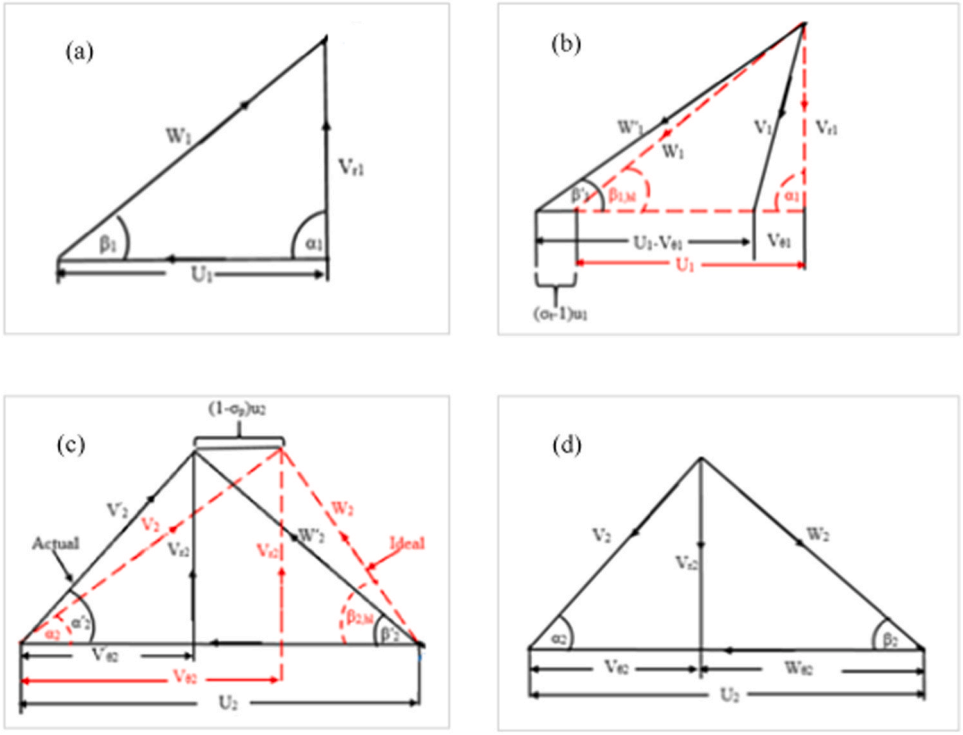

Fig. 1. The velocity triangles of pump inlet (a), PAT inlet (b), pump outlet (c), and PAT outlet (d) (Gülich, 2010).

the shock and diffusion losses at the impeller and volute were considered in the analysis.

2.1.1. Inlet losses

Hydraulic energy losses occur across all paths of the fluid passage, including the turbomachines' inlet and outlet sections. Flow disturbances, geometry, and flow conditions all have an impact on inlet losses. Since the pump inlet pipe functions as a PAT outlet, resulting in frictional loss, calculated as (Wang et al., 2020):

$$h_{\text{in,P}} = \left(\lambda\left(\frac{l_{\text{in}}}{D_{\text{e}}}\right)\left(\frac{V_0^2}{2g}\right)\right)_p \tag{1}$$

Where λ is the coefficient of friction, l_{in} the inlet length, D_{hy} is the inlet pipe hydraulic diameter, and V_o is the inlet pipe axial velocity, calculated as:

$$V_0 = \frac{Q}{\frac{\pi}{4}\left(D_1^2 \quad - D_{1\text{h}}^2\right)} \tag{2}$$

The friction coefficient was determined by the Reynolds number Re $= (\rho\ V_0\ D)/\mu$ *and* $\mu = 1.002 \times 10^{-3}$ *(N·s/m²)*, which is calculated using:

$$\lambda = \frac{0.3164}{\text{Re}^{1/4}} \text{for Re} < 10^6 \tag{3}$$

However, the pump inlet pipe, which acts as the PAT discharge, experiences friction loss, which calculated as follows:

$$h_{O,t} = \left(0.25\left(\frac{4Q}{\pi D_{\text{e}}^2}\right)^2 \frac{1}{2g} + \frac{V_{u1}^2}{2g}\right)_t \tag{4}$$

2.1.2. Impeller losses

Impeller losses account for more than half of the pump's total hydraulic losses (Qin et al., 2022). The PAT hydraulic loss deviates from the pump mode. The analysis considers inlet shock loss, skin friction loss, blade loading loss, and diffusion loss. The analysis uses the dimensional value and hydraulic diameter interchangeably, while other operational parameters are considered separately for each mode of operation.

1. **Shock loss in impeller**

The blade inlet flow angle equals the blade angle at the design flow rate, which prevents the occurrence of incidence loss. But when the flow rate changes from the design value, the fluid experiences a sudden change in velocity and direction as it passes through the impeller vanes. The abrupt change in direction can result in a change in flow angle, which causes shock waves and turbulence in the fluid. This causes flow separation and associated incidence loss. According to published data it has a value between 0.5 and 0.8 (Zaher, 2001).

$$h_{sh,La} = \left(C_{sh,La}\frac{\left(w_{1,p} - w_{1q,p}\right)^2}{2g}\right) \quad = \quad \left(C_{sh,La}\frac{(\Delta \text{w}_1)^2}{2g}\right) \tag{5}$$

where

$$\Delta w_1 = u_1\left(\frac{Q - Q_e}{Q_e}\right)_p \tag{6}$$

Researchers used other theoretical results based on assumptions in turbine mode to determine the best efficient point (Wang et al., 2020). In this work, the BEP from the CFD result was determined, and in a similar manner, the shock loss was determined as follows (Gülich, 2010):

$$h_{sh,La} = \left(C_{sh,La}\frac{\left(w_{2,t} - w_{2q,t}\right)^2}{2g}\right) \quad = \quad \left(C_{sh,La}\frac{(\Delta \text{w}_2)^2}{2g}\right) \tag{7}$$

where

$$\Delta w_2 = u_2\left(\frac{Q - Q_{BEP}}{Q_{BEP}}\right)_t \tag{8}$$

2. **Friction loss in impeller**

The friction loss $h_{fr,La}$ results from turbulent flow and shearing forces over impeller surface. This friction causes pressure loss, depending on the surface roughness and relative velocity. It follows the typical pipe friction loss (Tuzson, 2000). Both the pump and turbine modes of operation use the same formula. However, due to the difference in the flow phenomena, it yields a different value. Due to the irregular flow path across the impeller, the hydraulic diameter and average relative velocity were used (Gülich, 2010). Some of the authors of this work (Bantelay et al., 2024) developed a method to determine the detailed geometry of the pump.

$$h_{fr,La} = 4C_{fr,La}\left(\frac{l_b}{D_{hy,La}}\right)\left(\frac{w_{av}^2}{2g}\right) \tag{9}$$

Where the average relative velocity was determined as follows (Gülich, 2010):

$$D_{hy,La} = \frac{2(a_1b_1 + a_2b_2)}{(a_1 + b_1 + a_2 + b_2)} \tag{10}$$

$$w_{av} = \frac{2Q_{La}}{Z(a_1b_1 \quad + \quad a_2b_2)} \tag{11}$$

For laminar flow $Re_{La} < 10^5$:

$$C_{fr,La} = \frac{2.65}{\text{Re}_{La}^{\ 0.875}} - \frac{2}{8\text{Re}_{La} + \frac{0.016}{\text{Re}_{La}}} + \frac{1.328}{\sqrt{\text{Re}_{La}}} \tag{12}$$

For turbulent flow $10^5 < Re_{La} < 10^8$ and $0 < \varepsilon_{\text{La}}/l_b < 10^{-3}$: where the typical impeller roughness factor (ε_{La}) ranges from 0.001 to 0.01.

$$C_{fr,La} = \frac{0.136}{\left\{-\log\left(0.2\frac{\varepsilon_{La}}{l_b} + \frac{12.5}{\text{Re}_{La}}\right)\right\}^{2.15}} \tag{13}$$

$$\text{Re}_{La} = \frac{w_{av}l_b}{\nu} \tag{14}$$

3. **Blade loading loss in impeller**

Impeller blade loading loss refers to a decrease in the performance and efficiency of a centrifugal pump due to excessive loading on the impeller blades. Coppage et al., (Coppage and Dallenbach, 1956) equation with different operational parameters is used for both modes of operation to determine blade loading loss $h_{bl,La}$ and diffuser factor D_f as follows:

$$h_{bl,La} = 0.05\text{D}_f^{\ 2} \quad \frac{U_1^{\ 2}}{g} \tag{15}$$

$$D_f = 1 - \frac{w_1}{w_2} + \left(\frac{0.75 \quad gH_{th}}{u_1^2}\right) \quad \left(\frac{1}{\frac{z}{\pi}\left(1 - \frac{D_2}{D_1}\right) + \frac{2D_2}{D_1}}\right)\left(\frac{w_1}{w_2}\right) \tag{16}$$

4. **Separation loss in impeller**

A reverse pressure gradient and boundary layer loss along the flow direction cause impeller separation loss. This phenomenon can occur at

any location within the impeller. Most impeller and housing expansions in a pump occur suddenly. Separation occurs when the relative velocity ratio between the inlet and outlet fluids exceeds a critical value, typically around 1.4 (Tuzson, 2000). Therefore, the pump impeller diffusion loss was calculated as:

$$h_{df,La} = 0.25\frac{w_2^2}{2g} \tag{17}$$

In the PAT mode of operation, the throat part of the volute is unlikely to function as a contraction unit, allowing us to ignore the separation loss.

2.1.3. Volute losses

The pump's volute casing converts dynamic pressure to static pressure and leads it into the throat in pump mode, and the reverse is true for PATs. In PATs, the fluid enters the volute at an absolute velocity of V_3. This velocity is split into two components: a velocity parallel to the spiral (V_{3p}) and tangential to the impeller (V_{3d}) (El-Naggar, 2013). While in turbine mode, the volute casing plays an important role in converting the fluid's static pressure to dynamic pressure and directing it into the impeller. To determine the velocity components, it started with the inlet area and flow rate.

$$V_4 = \frac{Q}{A_4} \tag{18}$$

$$V_{3p} = \frac{V_4}{\cos\alpha_v} \tag{19}$$

$$V_{3d} = V_{u2} - V_4 \tag{20}$$

1. **Shock loss in volute**

The volute, similar to the impeller, encounters shock loss, also known as impact loss or incident loss, caused by the disparity between the volute inlet velocity V_3 and the volute through-flow velocity V_{3d} is estimated as (Tuzson, 2000):

$$h_{sh,v} = C_{sh}\frac{V_3^2 - V_{r2}^2}{2g} \tag{21}$$

While in PAT mode, the shock loss was evaluated as follows:

$$h_{sh,v} = C_{sh}\left(\frac{V_{3d}^2 - V_{3p}^2}{2g}\right) \tag{22}$$

2. **Friction loss in volute**

The volute friction loss was determined using the theory of flow through pipes as follows:

$$h_{fr,v} = 4C_{fr,v}\left(\frac{l_v}{D_{hy,v}}\right)\left(\frac{V_{3p}^2}{2g}\right) \tag{23}$$

The volute coefficient of friction is determined using the same calculation method as the impeller coefficient of friction, as described:

$$C_{fr,\ v} = \frac{2.65}{\mathrm{Re}_v^{0.875}} - \frac{2}{8\mathrm{Re}_v + \frac{0.016}{\mathrm{Re}_v}} + \frac{1.328}{\sqrt{\mathrm{Re}_v}} \tag{24}$$

The average Reynolds number and hydraulic diameter are calculated as follows:

$$Re_v = \frac{V_{3p}D_{hy,v}}{\nu} \tag{25}$$

$$D_{hy,v} = \frac{D_2}{\frac{1}{2(b_3/b_2)(D_3/D_2)} + \frac{1}{8(\pi/Z)(D_3/D_2)\sin(\alpha_v)}} \tag{26}$$

3. **Diffusion loss in volute**

Volute diffusion loss is caused by the volute rotational velocity $V_{3\,u}$. It is determined as:

$$h_{df,v} = C_D\frac{V_{3u}^2}{2g} \tag{27}$$

2.1.4. Throat losses

The pump throat plays a critical role in converting the fluid's velocity head to the pressure head before it enters the discharge piping. On the other hand, the process reverses when the pump functions as a turbine. During operation, however, the diffuser experiences both frictional and separation losses.

4. **Friction loss in throat**

The friction loss in the throat was determined as follows:

$$h_{f,th} = \frac{\lambda}{8\tan\left(\frac{\theta_{th}}{2}\right)}\left[\frac{D_{th}{}^2}{D_4{}^2} - 1\right]\frac{V_5^2}{2g} \tag{28}$$

Where

$$V_5 = \frac{Q}{A_{th}} \tag{29}$$

2.2. Performance analysis

2.2.1. Hydraulic efficiency

Euler's equation is a simplified mathematical equation that assumes a turbomachine has an infinitely thin blade. Therefore, the blade shape strictly governs fluid motion, exhibiting no swirling motion. Euler provides the ideal head for both modes of operation:

$$H_{\inf,p} = \left[\frac{(U_2V_{u2} - U_1V_{u1})}{g}\right]_p \tag{30}$$

$$H_{\inf,t} = \left[\frac{(U_1V_{u1} - U_2V_{u2})}{g}\right]_t \tag{31}$$

However, in practical situations, the impeller has a fixed number of blades with considerable thickness. Due to this, the relative and absolute velocities differed from Euler's ideal values. Therefore, the theoretical velocity components were calculated, considering the slip and blade blockage factors. Slipping only affects the tangential components of absolute and relative velocities, while blade blockage affects the flow velocity component. In PAT, slip occurs at the impeller's leading edge, unlike in pump mode. The absolute velocities of tangential components in pump and PAT modes were corrected by considering the slip factor as $V_{u2,p}{}' = \sigma_p V_{u2,p}$ in pump $V_{u1,t}{}' = \sigma_t V_{u1,t}$ and in PAT, respectively. Upon rearrangement, the theoretical head determined as follows:

$$H_{th,p} = \left[\frac{(U_2V_{u2}{}' - U_1V_{u1})}{g}\right]_p \tag{32}$$

$$H_{th,t} = \left[\frac{(U_1V_{u1}{}' - U_2V_{u2})}{g}\right]_t \tag{33}$$

$$V_{u2}{}' = u_2\left(\sigma_p - \frac{V_{2m}\tau_2}{u_2\tan\beta_{2B}}\right) \tag{34}$$

$$V_{u1}{}' = u_1\left(\sigma_t - \frac{V_{1r}\tau_1}{u_1\tan\beta_{1B}}\right) \tag{35}$$

The Stodola slip factor equation has been applied as follows (Dixon and Hall, 2013):

$$\sigma_p = \left(1 - \frac{\pi\sin\beta_{2b}}{Z}\right) \tag{36}$$

During the pump mode of operation, the fluid flow angle at the blade outlet is reduced compared to the blade's outlet angle due to the slip factor. However, in turbine mode, the fluid flow angle at the blade outlet exceeds the impeller blade angle. Consequently, the PAT slip factor (σt) is greater than 1 and determined by:

$$\sigma_t = \left(1 + \frac{\pi\sin\beta_{2b}}{Z}\right) \tag{37}$$

The blade blockage reduces the effective flow area and affects fluid flow through the impeller. It signifies the portion of fluid passage occupied by the blade thickness compared to an infinitely thin blade. It was determined:

$$\tau_1 = \left(1 - \frac{t_1 Z}{\pi D_1 \sin\beta_{1b}}\right)^{-1} \tag{38}$$

$$\tau_2 = \left(1 - \frac{t_2 Z}{\pi D_2 \sin\beta_{2b}}\right)^{-1} \tag{39}$$

Then, considering the hydraulic head losses, the real head was determined as:

$$H_{real,\ p} = H_{p,th} - h_{tot} \tag{40}$$

$$H_{real,\ t} = H_{p,th} + h_{tot} \tag{41}$$

$$h_{tot} = h_{in} + h_{La} + h_v + h_{th} \tag{42}$$

$$h_{La} = h_{shLa} + h_{blLa} + h_{frLa} + h_{DLa} \tag{43}$$

$$h_v = h_{shv} + h_{frv} + h_{Dv} \tag{44}$$

The hydraulic efficiency of the pump is determined in the following manner:

$$\eta_{h,p} = \left(\frac{H_{real}}{H_{th}}\right)_p \tag{45}$$

Then the PAT hydraulic efficiency determined as:

$$\eta_{h,t} = \left(\frac{H_{th}}{H_{real}}\right)_t \tag{46}$$

2.2.2. Volumetric efficiency

Fluid leakage between the rotating and fixed parts of the pump is due to the impeller inlet and outlet pressure differences. As a result, a portion of the impeller outlet flow rate returns through the gaps. This internal leakage (Q_L) causes losses of energy as the flow rate through the impeller,$(Q+Q_L)$ is increased compared to the useful flow rate Q. Then the volumetric efficiency (η_{vol}) was determined as:

$$\eta_{vol} = \frac{Q}{Q_{La}} = \frac{Q}{Q+Q_L} \tag{47}$$

$$Q_{La} = Q + Q_L = V_{r_2}\cdot\pi D_2 b_2 \varepsilon_2 \tag{48}$$

ε_2 is the blade thickness coefficient at the impeller outlet.

$$\varepsilon_2 = 1 - \left(\frac{Z}{\pi}\right)\left(\frac{\left(\frac{t_2}{\sin\beta_b}\right)}{D_2}\right) \tag{49}$$

Previous research output estimates the value of ε_2 to 0.95 (Logan, 2003).

2.2.3. Mechanical efficiency

Bearings and seals in turbomachinery cause mechanical energy loss. The pump's design determined this loss. Large pumps have higher mechanical efficiency. Small pumps, on the other hand, consume a significant portion of the power input. One can estimate the mechanical efficiency as follows (Mahieddine, 1987):

$$\eta_{me} = 1\Big/\left(1 + \frac{\eta_v\eta_h(P_{me}+P_{RR})}{\rho g H_{th} Q_{La}}\right) \tag{50}$$

From previous research, the mechanical power P_{me} loss due to the bearing accounts for 1 % of the useful power, and the power loss caused by disc friction P_{RR} between the impeller's rotating faces and the liquid was determined as follows (Gülich, 2010):

$$P_{RR} = \frac{k_{RR}}{\cos\delta}\rho\omega^3 R_2^5\left\{1 - \left(\frac{R_1}{R_2}\right)^5\right\} \tag{51}$$

$$h_{RR} = \frac{\frac{k_{RR}}{\cos\delta}\rho\omega^3 R_2^5\left\{1 - \left(\frac{R_1}{R_2}\right)^5\right\}}{\rho g Q} \tag{52}$$

Where P_{RR} is disc friction power loss, h_{RR} is disc friction head loss, ρ is the density of the fluid [kg/m^3], ω is the angular velocity, and δ is the deviation angle ($\delta = \beta_{2B} - \beta_2$) and, k_{RR} is an empirical friction coefficient presented in Table 3.

Where *Re* is Reynolds number ($\mathrm{Re} = uR/\nu = \omega R^2/\nu$), s_{ax} is the axial casing clearance $s_{ax}/R_2 = 0.035$ taken for this study. In this study, the mechanical efficiency was assumed at a constant 99.5 % across all ranges of operation. The researchers found that this value was sufficient for both the geometric assembly and the age of the machine under investigation.

2.3. Prediction procedure

Initially, hydraulic losses in the inlet pipe, impeller, volute, and throat caused by shock loss, friction loss, blade loading loss, and separation loss were considered. As a result, the volumetric losses due to leakage through clearances between the rotor and stator can be determined. Disc friction losses in the gaps between the rotor and stator are then measured, and efficiency and power output are calculated. Then, using the model presented below, a MATLAB syntax was developed to predict pump and turbine mode performance. Fig. 2 describes the modeling procedure. Initially, the operational and geometrical data were loaded. Then the velocity profile at the blade leading and trailing edges and the slip and blade blockage factors were determined. Then all hydraulic losses at the inlet, impeller, volute, and throat area are

Table 3
Friction coefficient (Daily and Nece, 1960).

Empirical friction coefficient	Range	Flow type
$k_{RR} = \frac{\pi R_2}{2Re s_{ax}}$	$\mathrm{Re}_{lam} \le 8.7(s_{ax}/R_2)^{-1.87}$	*Laminar and* merged boundary layers
$k_{RR} = \frac{0.925}{Re^{0.5}}\left(\frac{s_{ax}}{R_2}\right)^{0.1}$	$Re_{lam} < Re < 2\times10^5$	Laminar and separated boundary layers
$k_{RR} = \frac{0.02}{Re^{0.25}}\left(\frac{R_2}{s_{ax}}\right)^{1/6}$	$10^5 < Re < 10^6$	Turbulent and merged boundary layers
$k_{RR} = \frac{0.0255}{Re^{0.2}}\left(\frac{s_{ax}}{R_2}\right)^{0.1}$	$\mathrm{Re} > 2\times10^5$	Turbulent, separated boundary

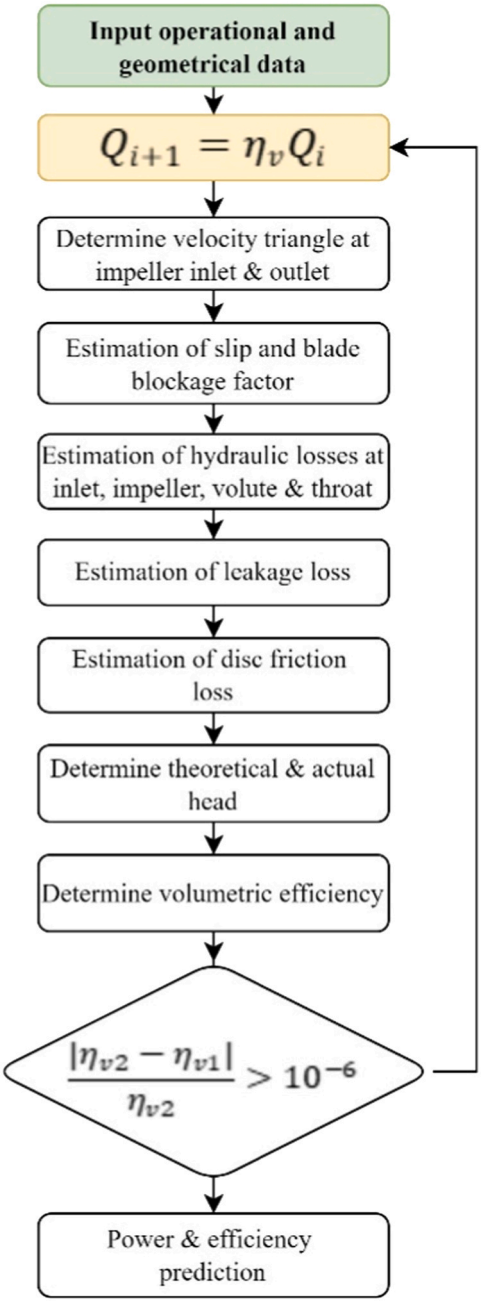

Fig. 2. MATLAB flow chart to predict PAT's performance using energy loss analysis.

estimated. Then theoretical and actual heads were determined, along with the pump's efficiency and power. Initially, the volumetric efficiency was assumed to commence the iterative loop and corrected through the iteration process. A stop condition is set for maintaining a minimal increase in volumetric efficiency over the entire range of flow rates. After determining the monomeric, hydraulic, mechanical, and volumetric efficiency, the overall efficiency calculated using the following formula:

$$\eta_o = \eta_v \eta_h \eta_m \tag{53}$$

In the numerical and experimental performance analysis, the head (H), torque (M), power (P), and efficiency (η) are determined as a function of height, static pressure, and average velocity as follows:

$$H = \left(z_1 + \frac{p_1}{\rho g} + \frac{v_1^2}{2g}\right) - \left(z_2 + \frac{p_2}{\rho g} + \frac{v_2^2}{2g}\right) \tag{54}$$

$$P = M \cdot \frac{2\pi n}{60} \tag{55}$$

$$\eta = \frac{\pi NM}{30 \rho g Q H} \times 100\% \tag{56}$$

2.4. Numerical modeling

2.4.1. Physical modeling

A computational fluid dynamics simulation was carried out to enable detailed insights into complex fluid flow phenomena inside the PAT. In this regard, proper physical modeling plays a tremendous role. Various CAD and non-CAD software programs are available to create industrial pump models. For centrifugal pumps, creating impeller and volute shapes can be time-consuming. ANSYS Blade Modular software provides an efficient method, known as BladeGen, for creating impeller blades with varying outlet angles. SolidWorks transfers three-dimensional pump geometry from CATIA to the ANSYS Design Modeler (DM) to maintain surface integrity and geometry accuracy. Fluent simulations avoid partition and shadow effects because of the model's meticulous modeling. To prevent abrupt changes, sharp edges and corners were smoothed out. The flow domain in which the detail geometry described in Table 2 was extracted and prepared for meshing is shown in Fig. 3.

2.4.2. Mesh generation

The computational grid generated on the flow domain. In turbine simulations, researchers have used various grid generation methods for pump operation. Most researchers used unstructured tetrahedral elements, while some researchers used both structured and unstructured elements in combination. Others have also utilized a combination of unstructured hexahedral and tetrahedral elements. Unstructured tetrahedral grids static mesh was generated using ANSYS-Workbench. To ensure grid quality, the patch-independent method is used.

2.4.3. Grid size and elements

To ensure the solution remains unaffected by changes in grid size, a grid convergence study with progressively finer grid resolutions was performed while keeping the time-step size constant. This test utilizes a patch-independent algorithm to refine the grid. Numerical simulations were conducted at various flow rates, specifically $0.5Q_{BEP}$, $0.6Q_{BEP}$, $0.8Q_{BEP}$, Q_{BEP}, $1.2Q_{BEP}$, $1.4Q_{BEP}$, $1.5Q_{BEP}$, and $1.6Q_{BEP}$. The dimensionless pressure drop coefficient (φ) is carefully monitored throughout these simulations. This coefficient represents the ratio of the actual pressure drop across the pump as a turbine to the pressure drop that would occur under ideal conditions without any losses. Table 4 displays the calculation results using the different grid numbers.

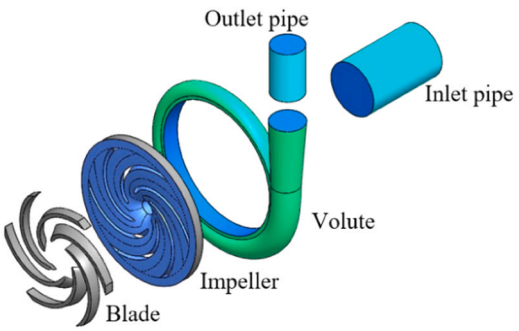

Fig. 3. Flow domain of the centrifugal pump.

Table 4
Computational grid independence test result.

No of elements	Dimensionless pressure drops coefficient							
	$0.5Q_d$	$0.6Q_d$	$0.8Q_d$	Q_d	$1.2Q_d$	$1.4Q_d$	$1.5Q_d$	$1.6Q_d$
4756,283	1.658	1.704	1.878	2.013	2.251	2.589	2.879	2.984
7183,090	***1.669***	***1.689***	***1.939***	***2.019***	***2.331***	***2.747***	***2.926***	***3.070***
12,303,012	1.679	1.677	1.990	2.025	2.397	2.878	2.964	3.141

$$\varphi = \frac{P_1 \quad - P_2}{0.5\rho u_2^2} \tag{57}$$

2.4.4. Verification of the computational study

The simulation for all cases has been run on a core i-7, 32 GB ram processor. To make sure each simulation results converged, all residuals were set to have 10^{-4}, and besides that, the solution-based criteria was used by monitoring the pressure drop coefficient computed from the solution. The solution has been monitored for the consecutive 1000 iterations, and the error was set to be 10^{-3}, hence each solution stopped when the difference between the last value fell below 10^{-3}.

To further validate the simulation, a grid independence study has been performed, for these three different grids. A mesh, which represents fine, medium, and coarse, was generated. This mesh was generated by altering the mesh element size by a factor of 1.5 for coarse, 1.25 for medium, and 0.8 for fine meshes. To validate the mesh, the Grid Convergence Index (GCI) is used to measure the accuracy and convergence of numerical solutions obtained from different grid sizes. It quantifies the error reduction achieved as the grid is refined. The GCI is determined using the following formula:

$$p = \ln\left(\frac{f_3 - f_2}{f_2 - f_1}\right) \Big/ \ln(r) \tag{58}$$

Where p is the order of convergence, r is the constant refinement ratio, f_3 is the pressure drops coefficient converge result for fine mesh, f_2 is the pressure drops coefficient converge result for medium mesh, and f_1 is the pressure drops coefficient converge result for coarse mesh. Then the grid convergence index (GCI) (Eça and Hoekstra, 2014) for the medium and fine refinement levels and defined as:

$$GCI = \frac{F_e|e|}{r^p - 1} \tag{59}$$

Hence, the calculated value of GCI is the asymptotic range of convergence by checking that $GCI \approx 1$. The results of the GCI calculations for each grid solution are listed in the following Table 5.

From Table 5, it can be shown that the difference between fine to medium mesh is about 0.21 %, whereas the difference between medium to coarse mesh is 0.95 %. Hence, the medium mesh size is selected to proceed with further simulation. The medium mesh scheme with 7183,090 mesh elements has been used to optimize computational costs.

2.4.5. Boundary conditions

The study uses the coupled pressure-velocity coupling method with a node-based gradient and second-order discretization to calculate pressure, momentum, kinetic energy, and dissipation rate. The frozen-rotor interface paradigm establishes a link between a rotating impeller and a stationary case, facilitating the exchange of flow information. The rotation was performed with multiple reference frame (MRF) in which steady state analysis were performed. To achieve realistic flow behavior, it implements non-slip boundary conditions and labels impeller, hub, and shroud walls as rotating and volute as stationary wall. Table 6 represents the boundary conditions of a pump operating as a turbine in water with a density of 998.2 kg/m3, a constant speed of 1450 RPM, an intensity of turbulence of 5 %, and an output boundary condition of 1 bar total pressure (Wei et al., 2023; Lin et al., 2021a; Štefan et al., 2020; Li et al., 2020; Rossi et al., 2019; Adu et al., 2019).

2.4.6. Turbulence model

Fluent offers various turbulence models for capturing turbulent behavior in centrifugal pumps. Researchers (Yang et al., 2012b; Frosina et al., 2017; Bai, X.) use two-equation models, such as standard k-ε SST turbulence models, to balance computational accuracy and effort in turbo-machinery applications. Most researchers (Wei et al., 2023; Lin et al., 2021a; Li et al., 2020; Adu et al., 2019; Jianguo et al., 2022) use the k-omega SST turbulence model, which incorporates transport effects in eddy viscosity formulation, is recommended for accurate prediction of flow separation onset and magnitude under adverse pressure gradients, making it the most suitable option in this study. The model predicts turbulence using two partial differential equations for k and ω, representing kinetic energy and a specific rate of dissipation. The study assumes an incompressible and steady flow field for stable long-term performance, incorporating peripheral velocity (u) as a parameter in the continuity equation.

Further, the study uses the best efficiency point values to normalize non-dimensional parameters. It includes the flow coefficient (ϕ), head coefficient (Ψ), specific speed (Ns), and power coefficient (Λ). This enables us to compare and evaluate performance in a meaningful way. The non-dimensional coefficients are set to determine BEP values. These parameters provide a comprehensive characterization of a turbomachine's behavior, defined as (Jain et al., 2015):

$$\phi = \quad Q/(\omega {D_2}^3) \tag{60}$$

$$\Psi = \quad 2gH/u_2^2 \tag{61}$$

$$\Lambda = P/\rho D_2^5 \omega^3 \tag{62}$$

Table 6
Boundary conditions used in the study.

PAT Boundary	Conditions
Inlet	Mass flow rate
Outlet	Total Pressure
Blades	Rotating wall
Impeller	Rotating wall
Casing	Stationary wall
Inlet Pipe	Stationary wall
Interface 1 (Between inlet pipe and impeller)	Fluid – fluid interface
Interface 2 (Between casing and impeller)	Fluid – fluid interface

Table 5
GCI calculation.

Parameter	f_3	f_2	f_1	P	GC12	GC23	Asymptotic range
pressure drops coefficient	1.679	1.669	1.658	0.18	0.21 %	0.95 %	1

$$N_s = N\frac{\sqrt{Q_e}}{H_e^{0.75}} \tag{63}$$

2.5. Experimental setup

Laboratory facility, set up as depicted in Fig. 4, to validate the model and computational results. At the thermo-fluid laboratory of Bahir Dar Institute of Technology at Bahir Dar University, a hydro-pump test rig was constructed to determine the efficiency, characteristics, and power curve and to gain a comprehensive understanding of the flow inside the machine. The accuracy and reliability of the analytical model and numerical simulation were validated using the test results. The laboratory setup allowed for the measurement of a set of performance-indicating parameters. The combination of analytical, numerical, and experimental work enhances the overall confidence in the results. The laboratory facility consists of essential components, including a service pump, a pump working as a turbine, an electromagnetic flow meter, a pressure sensor, customized hydraulic clamps, a flow-regulating valve, a bypass line, a reservoir, and a piping network. Wide-ranging data on pressure, flow rate, rotational speed, torque, and power across a wide range of flow rates was collected using this laboratory facility.

3. Results and discussion

In the analysis of PAT performance, the main factors, including the non-dimensional characteristics, power coefficient, and efficiency curves, were analyzed through analytical modeling, computational simulation, and experimentation. Fig. 5 shows the non-dimensional characteristic curve using the analytical model, CFD, and experiment results. A detailed investigation was carried out to identify BEP values to validate the accuracy of the models and computational results. Comparing the experimentally obtained BEP values, we observe that the PAT flow rate and head increase more than the BEP in pump mode, in line with the literature (Daily and Nece, 1960; Adu et al., 2019). Contrary to this, the overall efficiency of the PAT is slightly lower than that of the pump mode (Wei et al., 2023; Frosina et al., 2017). At BEP, the PAT produced 16.72 kW, 18.15 kW, and 17.9 kW of mechanical power using the analytical model, CFD, and experiment, respectively. Similarly, at BEP, the experimental result gives a 1.6 flow rate ratio and a 1.72 head ratio. In addition, Table 7 presents the detailed full flow performance results of the model, CFD, and experiment. All methods give a similar trend for most parameters.

Fig. 6 depicts a PAT's efficiency versus flow coefficient curve. The figure illustrates the ratio of the shaft's mechanical power to the fluid's input hydraulic power. According to the figure, the PAT has an efficiency of 76.53 %, 78.09 %, and 74.04 % using analytical, numerical, and experimental methods, respectively, at the BEP. The figure shows that PAT efficiency increases sharply up to a flow rate of 0.048 m3/s and a corresponding head of 46.48 m. Then it starts to decline smoothly beyond the BEP. This indicates that it is preferable to use PAT at greater off-design flow rate compared to a lower flow rate. The finding of Rossi et al (Rossi et al., 2019). is also concurred with.

The experimental efficiency is lower than both the model and the numerical efficiency. At BEP, the deviations from the experimental results are −2.04 % and 3.08 % for the CFD and analytical results, respectively. Which is more accurate than other results (Rossi et al., 2019). In the model, the deviation might come from neglecting minor losses such as wake mixing and recirculation losses and computation error, whereas in the numerical simulation, it might come from negligence of leakage and mechanical losses. In the CFD analysis, impeller clearance has been neglected. Therefore, the numerical results do not consider the volumetric losses due to the leakages passing through the gaps between the impeller and the volute casing. Furthermore, the numerical analysis does not consider the mechanical friction losses caused by the shaft and bearing rotation. The change trends for the analytical model, CFD, and experimental efficiency curves are identical, and the results are consistent with the experimental data. Therefore, this study's analytical model and numerical simulation results agreed with the experimental result. Further, the energy loss analysis was carried out by combining the analytical models with numerical simulation.

Table 8 presents the percentage relative difference between the numerical and analytical results with an experimental value. The CFD results encountered a maximum relative difference of 3.90 %, 1.36 %, and 5.47 % for the head coefficient, power coefficient, and efficiency at the BEP, and a decrease as it moved away from the BEP of the PAT. Whereas the model results encountered a relative difference of 9.66 %, 6.63 %, and 3.36 % for the head coefficient, power coefficient, and efficiency at the BEP. It is in good agreement with others findings (Stefanizzi et al., 2017; Rossi et al., 2019; Lin et al., 2021b; Liu et al., 2022, 2019b). In general, PAT's head coefficient shows a decreasing trend as it moves away from a higher flow coefficient. Whereas the power coefficient shows an inverse trend with the head coefficient for both methods. The results are in reasonable agreement with other researcher's output. In general, the percentage relative error of efficiency near the PAT's best efficient point is small enough as compared to being far apart from the BEP, as depicted by other's findings (Barbarelli et al., 2016; Ştefan et al., 2020; Rossi et al., 2019).

The head coefficient, power coefficient, and efficiency are the most important parameters in selecting a pump for PAT application and proper operation. The head coefficient represents the ratio of the effective head available to generate power to the total head from the potential energy of the water. Similarly, the power coefficient represents the ratio of the turbine's actual power output to the maximum possible power output from the available water energy. After incorporating the correction factor, the analytical results were used to develop an analytical method to predict these parameters. An analytical method

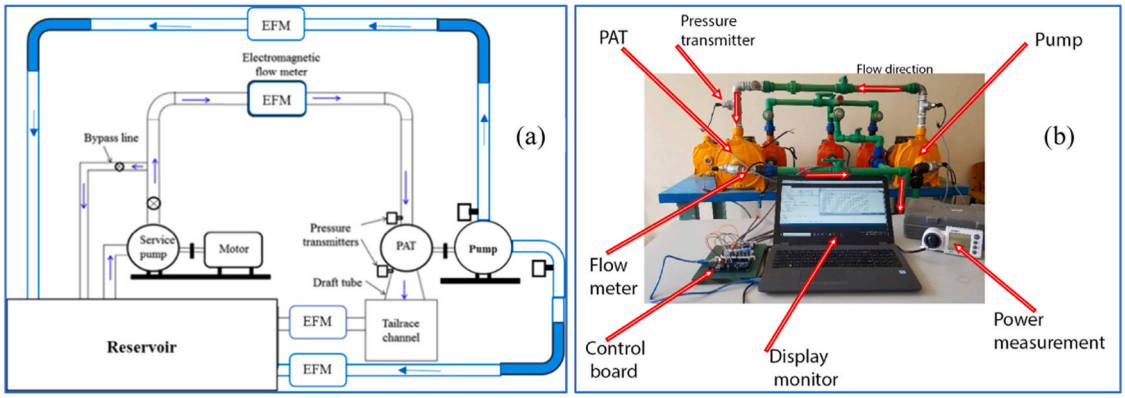

Fig. 4. A schematic drawing of the experimental setup (a) and a picture of the setup in the lab (b).

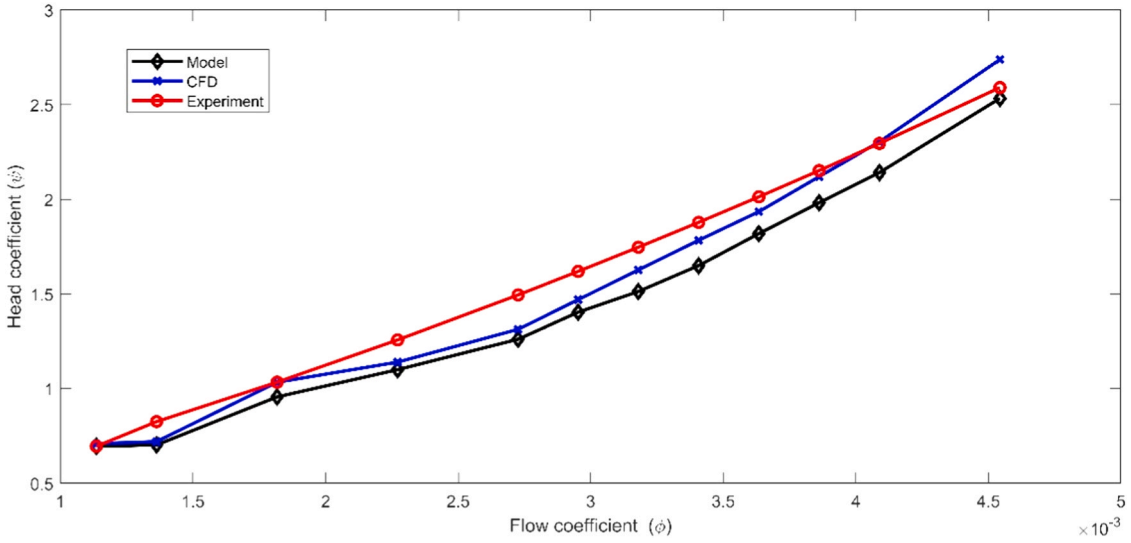

Fig. 5. PAT characteristics curve using model, CFD and experiment.

Table 7
Performance of PAT using experiment, CFD and model.

Flow coefficient ϕ	Experiment			CFD			Model		
	Head coefficient ψ	*Power coefficient* Λ	*Efficiency* η	*Head* coefficient ψ	*Power coefficient* Λ	*Efficiency* η	*Head* coefficient ψ	*Power coefficient* Λ	*Efficiency* η
0.0011	0.70	0.0001	41.91	0.71	0.0001	42.75	0.69	0.0001	41.90
0.0014	0.83	0.0002	51.43	0.72	0.0002	53.47	0.70	0.0002	52.40
0.0018	1.03	0.0005	61.72	1.03	0.0004	54.55	0.96	0.0004	53.46
0.0023	1.26	0.0012	67.77	1.14	0.0011	71.27	1.10	0.0011	69.84
0.0027	1.50	0.0015	71.30	1.31	0.0014	75.65	1.26	0.0013	74.14
0.0030	1.62	0.0015	72.43	1.47	0.0014	74.98	1.40	0.0013	73.48
0.0032	1.75	0.0017	73.25	1.63	0.0017	76.87	1.51	0.0015	75.33
0.0034	1.88	0.0020	73.81	1.78	0.0020	78.03	1.65	0.0018	76.47
0.0036	***2.01***	***0.0023***	***74.04***	***1.94***	***0.0023***	***78.09***	***1.82***	***0.00214***	***76.53***
0.0039	2.15	0.0026	73.81	2.12	0.0027	77.98	1.98	0.0025	76.42
0.0041	2.29	0.0029	73.43	2.30	0.0031	77.39	2.14	0.0028	75.84
0.0045	2.59	0.0036	73.02	2.74	0.0039	74.30	2.53	0.0036	72.81

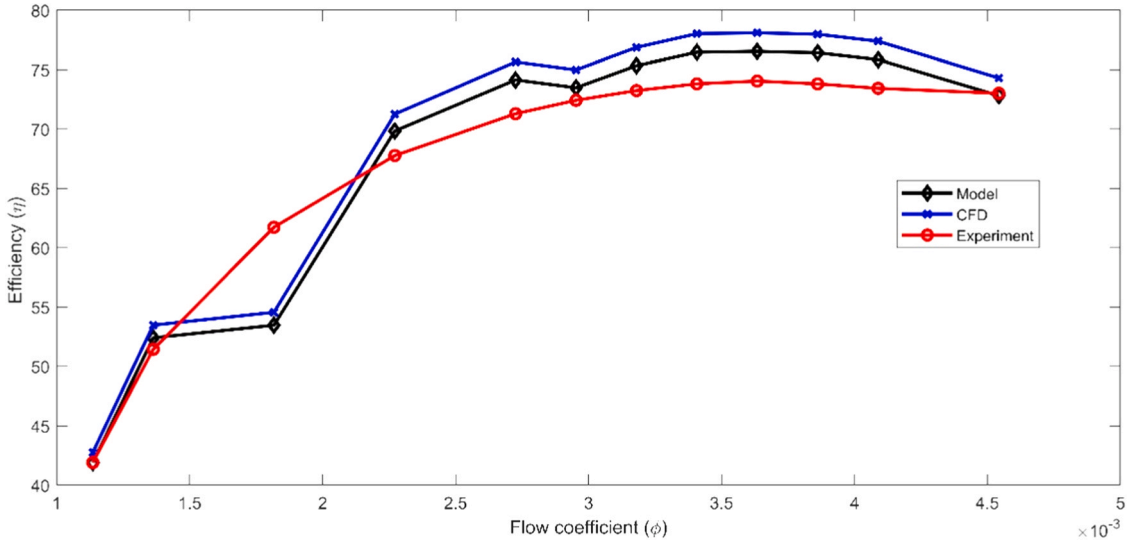

Fig. 6. PAT efficiency curve for model, CFD and experiment.

proposed to predict the head coefficient of the PAT is presented as follows:

$$\psi(\phi) = 34910\phi\hat{}2 + 348.8*\phi + 0.2853 \quad (64)$$

Whereas the proposed model to predict the power coefficient of the PAT is described as follows:

Table 8
Percentage relative difference between numerical and analytical results with experimental value.

Flow coefficient φ	Numerical			Model		
	Head coefficient Δψ (%)	Power coefficient ΔΛ (%)	efficiency Δη (%)	Head coefficient Δψ (%)	Power coefficient ΔΛ (%)	efficiency Δη (%)
0.0011	-2.03	-4.09	-2.02	0.01	0.03	0.02
0.0014	12.75	9.29	-3.97	14.93	13.33	-1.89
0.0018	0.05	11.67	11.62	7.55	19.93	13.39
0.0023	9.33	6.79	-5.16	12.51	12.31	-3.06
0.0027	12.15	6.03	-6.11	15.67	12.05	-3.98
0.0030	9.23	6.03	-3.52	13.31	12.05	-1.45
0.0032	6.87	2.26	-4.95	13.39	10.92	-2.85
0.0034	5.05	-0.37	-5.71	12.17	9.02	-3.60
0.0036	**3.90**	**-1.36**	-5.47	**9.66**	**6.63**	-3.36
0.0039	1.49	-4.07	-5.65	7.89	4.64	-3.53
0.0041	-0.37	-5.78	-5.39	6.66	3.59	-3.28
0.0045	-5.72	-7.58	-1.76	2.21	2.48	0.28

$$\Lambda(\phi) = 63900\phi\hat{}3 - 399.2\phi\hat{}2 + 1.588\,\phi - 0.001294 \quad (65)$$

Similarly, the proposed model to predict the efficiency of the PAT is given as:

$$\eta(\phi) = 149.2\phi\hat{}3 - 177{*}e\hat{}5{*}\phi\hat{}2 + 6.978e{+}04{*}\phi + -10.49 \quad (66)$$

Detailed investigations were conducted using these models to thoroughly examine the losses in turbine modes, analyzing the variations of each loss with respect to the flow rate. Table 9 presents the characteristics, specific trends, and patterns of loss variations. Volute frictional loss (12.1 %), throat friction loss (11.9 %), inlet pipe friction loss (11.2 %), impeller friction loss (9.4 %), and volute diffusion loss (8.9 %) contribute dominantly in a sequence at the BEP. The result provides valuable insights into the performance of the system under different operating conditions and is alien to others (Barbarelli et al., 2016; Liu et al., 2019b).

Fig. 7 shows the percentage of energy loss in each part. The PAT has 18.17 % of an inlet pipe, 17.75 % of impeller loss, 44.75 % of volute, and 19.33 % throat losses. At BEP the PAT energy loss basically comes from the pump volute loss. Other losses have a similar effect on the average. As pumps are designed for pressurizing service they don't have flow control device like conventional turbines. This insisted them for high loss as flow rate increase. However, if the PAT operates at the pump design flow rate, it will account for 41.31 % of impeller loss. The study expressed that, in general, as flow rates increase, inlet pipe and impeller losses decrease. In contrast, volute and throat losses increase as flow rates increase.

Like the performance prediction model, the analytical results were used to develop an average energy share at the inlet pipe, impeller, volute, and throat. An analytical method proposed to predict the inlet pipe loss share of the PAT is presented as follows:

$$h_{in}(\%) = 5.5x10^{8}\phi^{3} - 6.1x10^{6}\phi^{2} + 1.6x10^{4}\phi + 16 \quad (67)$$

Whereas the proposed model to predict the impeller loss share of the PAT is described as follows:

$$h_{La}(\%) = 1.5x10^{9}\phi^{3} - 8.8x10^{6}\phi^{2} - 4.2x10^{3}\phi + 79 \quad (68)$$

Similarly, the proposed model to predict the volute loss share of the PAT is given as:

$$h_{v}(\%) = -1.3x10^{9}\phi^{3} + 9.4x10^{6}\phi^{2} - 5x10^{3}\phi + 2.3 \quad (69)$$

Finaly, the proposed model to predict the throat loss share of the PAT is given as:

$$h_{throat}(\%) = -6.8x10^{8}\phi^{3} + 5.6x10^{6}\phi^{2} - 6.7x10^{3}\phi + 3.2 \quad (70)$$

For a better visual understanding of the energy loss analysis, contour maps were developed and presented using the case pump running at 36 kg/s. Fig. 8 presents the wall shear stress contour in a pump impeller and volute. The fluid exerts tangential stress on the wall, a measure of wall shear stress. It represents the frictional forces that the fluid experiences as it flows through the pump impeller. It demonstrates that the PAT has regions with high frictional losses. These regions are typically associated with high-velocity gradients or flow separation, where the

Table 9
Percentage energy loss analysis.

Flow rate Q [m^3/s]	Inlet pipe friction losses (h_{in}) – [%]	Impeller Shock loss ($h_{sh,La}$) – [%]	Impeller Friction loss ($h_{fr,La}$) – [%]	Impeller Blade loading loss ($h_{bl,La}$) – [%]	Impeller Separation loss ($h_{d,La}$) – [%]	Total impeller loss	Volute Shock loss ($h_{sh,v}$) – [%]	Volute Friction loss ($h_{fr,v}$) – [%]	Volute Diffusion loss ($h_{d,v}$) – [%]	Total Volute loss ($h_{v,total}$) – [%]	Throat Friction loss ($h_{f,th}$) – [%]
0.015	15.5	5.5	11.1	1.1	20.0	37.6	0.6	2.8	0.7	4.1	1.1
0.018	15.9	4.8	11.5	1.2	18.1	35.6	0.9	3.6	1.1	5.6	1.6
0.021	16.1	4.2	11.9	1.3	16.0	33.4	1.3	4.6	1.6	7.5	2.3
0.024	16.2	3.5	12.2	1.3	13.8	30.8	1.7	5.6	2.2	9.6	3.1
0.027	16.1	2.8	12.3	1.4	11.5	27.9	2.2	6.7	3.0	11.9	4.1
0.03	15.9	2.1	12.3	1.4	9.2	25.0	2.9	7.8	3.8	14.4	5.2
0.033	15.5	1.5	12.2	1.5	7.0	22.0	3.5	8.8	4.7	17.0	6.4
0.036	14.9	1.0	11.9	1.5	5.0	19.2	4.1	9.8	5.6	19.5	7.6
0.039	14.1	0.6	11.4	1.5	3.3	16.6	4.8	10.6	6.4	21.9	8.8
0.042	13.2	0.2	10.8	1.4	1.9	14.3	5.5	11.3	7.3	24.1	9.9
0.045	12.2	0.1	10.1	1.4	0.9	12.4	6.1	11.7	8.1	26.0	11.0
0.048	***11.2***	***0.0***	***9.4***	***1.3***	***0.3***	***10.9***	***6.6***	***12.1***	***8.9***	***27.5***	***11.9***
0.051	10.2	0.1	8.6	1.2	0.0	9.8	7.1	12.2	9.5	28.7	12.6
0.054	9.2	0.2	7.8	1.2	0.1	9.2	7.5	12.2	9.9	29.6	13.3
0.057	8.2	0.4	7.0	1.1	0.4	8.8	7.8	12.1	10.3	30.2	13.8
0.06	7.4	0.7	6.3	1.0	0.8	8.8	8.0	11.9	10.6	30.5	14.1

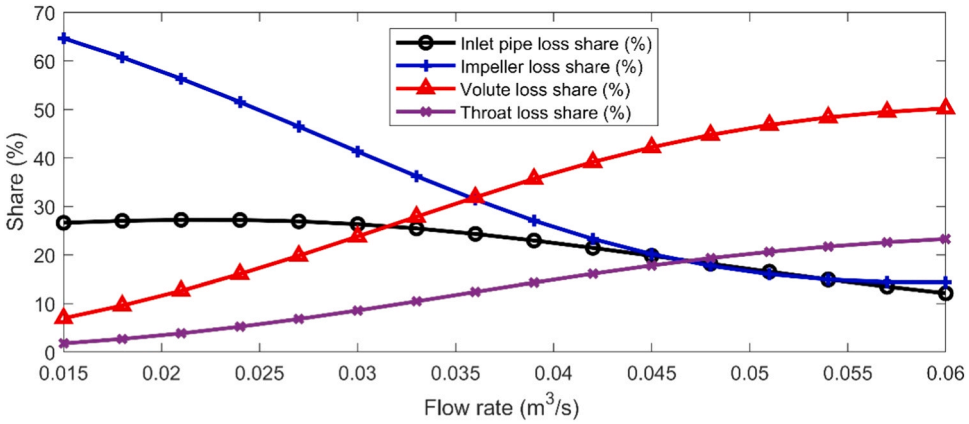

Fig. 7. Percentage of energy loss by part.

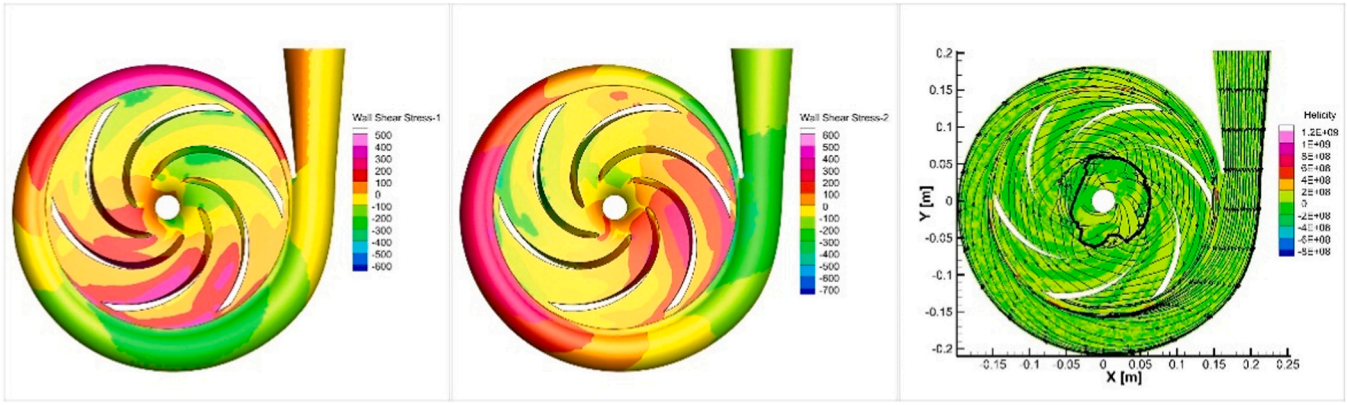

Fig. 8. presents the wall shear stress and stream line contours in a pump impeller and volute.

fluid experiences significant frictional resistance.

Fig. 9 depicts the static pressure contour of a pump impeller and volute. A maximum of 2.214 MPa and a minimum of −0.6 MPa were observed over the blade's surface. Excessive pressure variations or non-uniform pressure distribution on the impeller blades, as shown in the contours, cause blade loading loss, which manifests as high blade loading loss in a PAT. As shown in the figure, the pressure distribution on the impeller and volute identifies regions of high or low pressure. Non-uniform pressure distribution leads to imbalanced loading on the blades, resulting in increased on blade loading and associated losses and reduced efficiency.

Fig. 10 presents the velocity magnitude contours of a pump impeller and volute. The spreading out of fluid velocity as it passes through the pump causes a decrease in pump performance, known as diffusion loss. The velocity magnitude contour illustrates the distribution of fluid velocity within the impeller and the corresponding diffusion loss. Areas of decreasing or spreading velocity indicate a decrease in kinetic energy and an increase in energy losses.

4. Conclusion

In this study, the non-dimensional characteristics, power coefficient, and efficiency curves were analyzed through energy loss analysis, and simple and accurate prediction models were developed. at BEP, the PAT produced 16.72 kW, 18.15 kW, and 17.9 kW of mechanical power using the model, CFD, and experiment results, respectively. Similarly, the experimental result gives a 1.6 flow rate ratio and a 1.72 head ratio. Comparing the experimentally obtained BEP values, we observe that the

Fig. 9. The figure depicts the static pressure distribution contour over the pump impeller and volute.

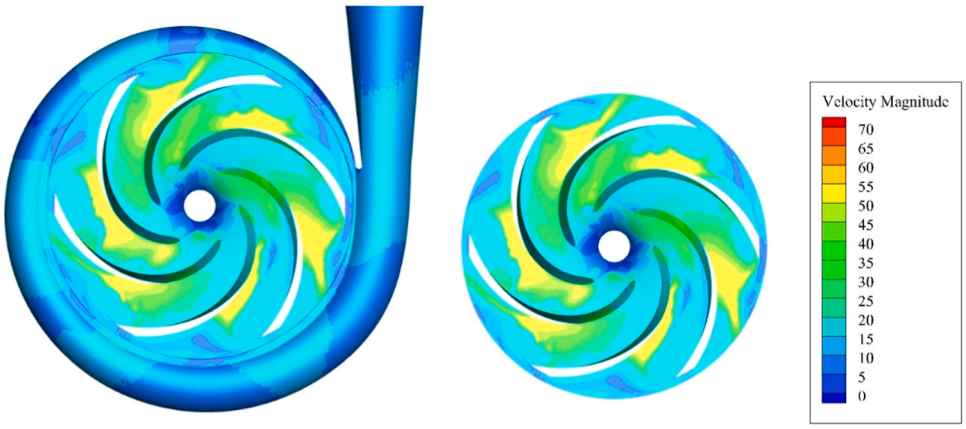

Fig. 10. Velocity magnitude contour over the pump impeller and volute.

PAT flow rate and head increase more than the BEP in pump mode. While the PAT's overall efficiency is slightly lower than that of the pump mode. Moreover, the PAT efficiency increases sharply up to a flow rate of 0.048 m3/s and a corresponding head of 46.48 m. Then it starts to decline smoothly. It has an efficiency of 76.53 %, 78.09 %, and 74.04 % using analytical, numerical, and experimental methods, respectively, at the BEP. The change trends for the analytical model, CFD, and experimental efficiency curves are identical, and the results are consistent with the experimental data. Moreover, the result indicates that using PAT at higher off-design is second priority next to BEP compared to a lower one. The experimental efficiency is lower than both the model and the numerical efficiency. At BEP, the deviations from the experimental results are −2.04 % and 3.08 % for the CFD and analytical results, respectively. This accuracy surpasses that of previous findings.

The CFD results provide a percentage relative difference with an experimental value of 3.90 %, 1.36 %, and 5.47 % for the head coefficient, power coefficient, and efficiency at the BEP, and a decrease as it moves away from the BEP of the PAT. Whereas the model gives a percentage relative difference with an experimental value of 9.66 %, 6.63 %, and 3.36 % for the head coefficient, power coefficient, and efficiency relative difference at the BEP. In general, PAT's head coefficient shows a decreasing trend as it moves to a higher flow coefficient. While the power coefficient shows an inverse trend for both methods, it is in good agreement with previous findings, which relied on different methods.

Detailed energy loss investigations were conducted using developed models to thoroughly examine the variations of each loss with respect to the flow rate. Table 9 presents the characteristics, specific trends, and patterns of loss variations. Volute frictional loss (12.1 %), throat friction loss (11.9 %), inlet pipe friction loss (11.2 %), impeller friction loss (9.4 %), and volute diffusion loss (8.9 %) contribute dominantly in a sequence at the BEP. The PAT encountered 18.17 % of an inlet pipe loss, 17.75 % of impeller loss, 44.75 % of volute loss, and 19.33 % of throat loss. However, if the PAT operates at the pump design flow rate, it will account for 41.31 % of impeller loss. The study exposed that, in general, as flow rates increase, inlet pipe and impeller losses decrease. In contrast, volute and throat losses increase as flow rates increase. The result provides valuable insights into each loss variation under different operating conditions and points out the special areas of focus to undertake design improvement and operational optimization.

We developed and presented the wall shear stress, static pressure, and velocity magnitude contour maps using a case pump running at 36 kg/s to enhance the visual understanding of the energy loss analysis. The wall shear stress contour demonstrates that the PAT has regions with high frictional losses. These regions are typically associated with flow separation, where the fluid experiences significant frictional resistance. Likewise, the static pressure contour exhibits a non-uniform pressure distribution ranging from a maximum of 12 MPa to a minimum of −0.6 MPa over the blade's surface, causing blade loading loss, which manifests as high blade loading loss in a PAT. Equally, the velocity and magnitude contours of high diffusion of fluid velocity as it passes through the pump cause a diffusion loss.

Overall, the study provides a valuable insight into the performance and detail of energy loss variation across a wide range of operations, which narrows the research limitations in the area. Furthermore, the proposed prediction models provide accurate energy loss estimations that surpass the accuracy of previous findings. However, more research is required to understand the causes of the model's deviation, considering minor losses like wake mixing and recirculation losses, as well as computation error.

Authorship statement

Manuscript Title: " ***Performance prediction of a pump as a turbine using energy loss analysis*****"** All persons who meet authorship criteria are listed as authors, and all authors certify that they have participated sufficiently in the work to take public responsibility for the content, including participation in the concept, design, analysis, writing, or revision of the manuscript. Furthermore, each author certifies that this material or similar material has not been and will not be submitted to or published in any other publication before its appearance in the ***Energy***

CRediT authorship contribution statement

Girma Gebresenbet: Supervision, Investigation. **Muluken Zegeye:** Writing – review & editing, Supervision, Methodology, Formal analysis, Conceptualization. **Bimrew Tamrat:** Writing – review & editing, Supervision, Methodology, Conceptualization. **Muluken Temesgen:** Writing – review & editing, Software, Methodology, Formal analysis, Data curation. **Dessie Tarekegn Bantelay:** Writing – review & editing, Writing – original draft, Visualization, Validation, Software, Methodology, Investigation, Formal analysis, Data curation, Conceptualization.

Declaration of Competing Interest

The authors declare that they have no known competing financial interests or personal relationships that could have appeared to influence the work reported in this paper

Data availability

Data will be made available on request.

Acknowledgments

All persons who have made substantial contributions to the work reported in the manuscript (e.g., technical help, writing and editing assistance, general support), but who do not meet the criteria for authorship, are named in the Acknowledgements and have given us their written permission to be named. If we have not included an acknowledgment, then that indicates that we have not received substantial contributions from non-authors.

References

Li, X.-z, et al., 2018. Hydropower development situation and prospects in China. Renew. Sustain. Energy Rev. 82, 232–239. https://doi.org/10.1016/j.rser.2017.08.090.

Binama, M., et al., 2017. Investigation on pump as turbine (PAT) technical aspects for micro hydropower schemes: a state-of-the-art review. Renew. Sustain. Energy Rev. 79, 148–179. https://doi.org/10.1016/j.rser.2017.04.071.

Barbarelli, S., Amelio, M., Florio, G., 2016. Predictive model estimating the performances of centrifugal pumps used as turbines. Energy 107, 103–121. https://doi.org/10.1016/j.energy.2016.03.122.

Muttalli, R.S., Agrawal, S., Warudkar, H., 2014. CFD simulation of centrifugal pump impeller using ANSYS-CFX. Int. J. Innov. Res. Sci., Eng. Technol. 3 (8), 15553–15561 https://core.ac.uk/download/pdf/357380307.pdf.

Thoma, D., Kittredge, C., 1931. Centrifugal pumps operated under abnormal conditions. Power 73, 881–884.

Popescu, D., Duinea, A., Rusinaru, D., 2013. Study of centrifugal pump operating as turbine in small hydropower plants. Recent Res. Electr. Power Energy Syst. 285–288.

Giosio, D., et al., 2015. Design and performance evaluation of a pump-as-turbine micro-hydro test facility with incorporated inlet flow control. Renew. Energy 78, 1–6. https://doi.org/10.1016/j.renene.2014.12.027.

Derakhshan, S., Nourbakhsh, A., 2008. Experimental study of characteristic curves of centrifugal pumps working as turbines in different specific speeds. Exp. Therm. Fluid Sci. 32 (3), 800–807.

Orchard, B., Klos, S., 2009. Pumps as turbines for water industry. World Pumps 2009 (8), 22–23.

Buse, F., 1981. Using centrifugal pumps as hydraulic turbines. Chem. Eng. 88, 113–117.

Bantelay, D.T., 2019. Investigating water supply system electro-mechanical equipments problems: a case study of Ethiopia. J. Optim. Ind. Eng. 12 (2), 45–54.

Motwani, K., Jain, S., Patel, R., 2013. Cost analysis of pump as turbine for pico hydropower plants–a case study. Procedia Eng. 51, 721–726. https://doi.org/10.1016/j.proeng.2013.01.103.

Raman, N., et al., 2013. An experimental investigation of pump as turbine for micro hydro application. in IOP conference series: Earth and environmental science. IOP Publishing. https://doi.org/10.1088/1755-1315/16/1/012064.

Chappallaz, J., *Manual on Pumps Used as Turbines, 1992*. Google Scholar, 1992.

Stepanoff, A.J., 1957. Centrif. axial Flow. Pumps.: Theory, Des., Appl. https://cir.nii.ac.jp/crid/1573387449864191104.

Yang, S.-S., Derakhshan, S., Kong, F.-Y.J.R.E., 2012a. Theoretical, numerical and experimental prediction of pump as turbine performance. Renew. Energy 48, 507–513. https://doi.org/10.1016/j.renene.2012.06.002.

Sharma, K.J.K.E.C., Bangalore, India, *Small hydroelectric project-use of centrifugal pumps as turbines*. 1985.

Singh, P., Nestmann, F.J.E.T., Science, F., 2010. An optimization routine on a prediction and selection model for the turbine operation of centrifugal pumps. Exp. Therm. Fluid Sci. 34 (2), 152–164. https://doi.org/10.1016/j.expthermflusci.2009.10.004.

Derakhshan, S., Nourbakhsh, A.J.Et, science, f, 2008. Theoretical, numerical and experimental investigation of centrifugal pumps in reverse operation. Exp. Therm. Fluid Sci. 32 (8), 1620–1627. https://doi.org/10.1016/j.expthermflusci.2008.05.004.

Nautiyal, H., et al., 2011. Experimental investigation of centrifugal pump working as turbine for small hydropower systems. Energy Sci. Technol. 1 (1), 79–86.

Williams, A.J.PotIo.M.E., 1994. Part A:, the turbine performance of centrifugal pumps: a comparison of prediction methods. J. Power Energy 208 (1), 59–66 https://journals.sagepub.com/doi/10.1243/PIME_PROC_1994_208_009_02.

Liu, M., Tan, L., Cao, S.J.E., 2019a. Theoretical model of energy performance prediction and BEP determination for centrifugal pump as turbine. Energy 172, 712–732. https://doi.org/10.1016/j.energy.2019.01.162.

Childs, S.M., 1962. Convert pumps to turbines and recover HP. Hydrocarb. Process. Pet. ReJner 41 (10).

Hancock, J.W., 1963. Centrifugal pump or water turbine. Pipe Line N. 25–27.

McClaskey, B.Ma.L., J.A.., *Hydraulic power recovery turbines.* ASME Conference, 1976 (paper 76-Pet-65).

Grover, K.M., 1980. Conversion of pumps to turbines. GSA Inter Corp, Katonah, New York.

Schmiedl, E., *Serien-Kreiselpumpen im Turbinenbetrieb.* Pumpentagung: Karlsruhe, Germany, 1988.

Alatorre-Frenk, C., Thomas, T.H., 1990. The pumps as turbines approach to small hydropower. In: In World Congress on Renewable Energy, Proceedings of the 1st World Renewable Energy Congress, **5**. Pergamon Press, pp. 2914–2918.

Jain, S.V., Swarnkar, A., Motwani, K.H., Patel, R.N., 2015. Effects of impeller diameter and rotational speed on performance of pump running in turbine mode. Energy Convers. Manag. 89, 808–824. https://doi.org/10.1016/j.enconman.2014.10.036.

Tan, X., Engeda, A., 2016. Performance of centrifugal pumps running in reverse as turbine: Part II-systematic specific speed and specific diameter based performance prediction. Renew. Energy 99, 188–197. https://doi.org/10.1016/j.renene.2016.06.052.

Stefanizzi, M., et al., 2017. Experimental investigation and performance prediction modeling of a single stage centrifugal pump operating as turbine. Energy Procedia 126, 589–596. https://doi.org/10.1016/j.egypro.2017.08.218.

Fontanella, S., et al., 2020. A performance prediction model for pumps as turbines (PATs). Water 12 (4), 1175. https://doi.org/10.3390/w12041175.

Kara Omar, A., Khaldi, A., Ladouani, A., 2017. Prediction of centrifugal pump performance using energy loss analysis. Aust. J. Mech. Eng. 15 (3), 210–221. https://doi.org/10.1080/14484846.2016.1252567.

Yang, S.-S., Derakhshan, S., Kong, F.-Y., 2012b. Theoretical, numerical and experimental prediction of pump as turbine performance. Renew. Energy 48, 507–513.

Wang, L., et al., 2020. Geometrical optimization of pump-as-turbine (PAT) impellers for enhancing energy efficiency with 1-D theory. Energies 13 (16), 4120. https://doi.org/10.3390/en13164120.

Ghorani, M.M., et al., 2020. A numerical study on mechanisms of energy dissipation in a pump as turbine (PAT) using entropy generation theory. Renew. Energy 162, 1036–1053. https://doi.org/10.1016/j.renene.2020.08.102.

Li, D., et al., 2017. Entropy production analysis of hysteresis characteristic of a pump-turbine model. Energy Convers. Manag. 149, 175–191. https://doi.org/10.1016/j.enconman.2017.07.024.

Xin, T., et al., 2022. Analysis of hydraulic loss of the centrifugal pump as turbine based on internal flow feature and entropy generation theory. Sustain. Energy Technol. Assess. 52, 102070 https://doi.org/10.1016/j.seta.2022.102070.

Yu, A., et al., 2022. Numerical study on the energy evaluation characteristics in a pump turbine based on the thermodynamic entropy theory. Renew. Energy 195, 766–779. https://doi.org/10.1016/j.renene.2022.06.077.

Zhou, L., et al., 2022. Application of entropy production theory for energy losses and other investigation in pumps and turbines: A review. Appl. Energy 318, 119211. https://doi.org/10.1016/j.apenergy.2022.119211.

Dixon, S.L., Hall, C., 2013. Fluid mechanics and thermodynamics of turbomachinery. Butterworth-Heinemann.

Gülich, J.F., 2010. Turbine operation, general characteristics. in Centrifugal Pumps. Springer Berlin Heidelberg, Berlin, Heidelberg, pp. 715–740. https://doi.org/10.1007/978-3-642-12824-0_12.

Bantelay, D.T., et al., 2024. One-dimensional pump geometry prediction modeling for energy loss analysis of pumps working as turbines. Int. J. Thermofluids, 100562. https://doi.org/10.1016/j.ijft.2024.100562.

Qin, Y., et al., 2022. Investigation on hydraulic loss component and distribution in hydraulic machinery: A case study of pump-turbine in pump mode. J. Energy Storage 52, 104932. https://doi.org/10.1016/j.est.2022.104932.

Zaher, M.J.PotIo.M.E., 2001. Part E:, approximate method for calculating the characteristics of a radial flow pump. J. Process Mech. Eng. 215 (4), 295–316. https://doi.org/10.1177/095440890121500404.

Tuzson, J., 2000. Centrifugal pump design. John Wiley & Sons.

Coppage, J., Dallenbach, F., 1956. Study of supersonic radial compressors for refrigeration and pressurization systems. Garrett Corp Los Angeles Ca AiResearch MFG DIV.

El-Naggar, M.A., 2013. A one-dimensional flow analysis for the prediction of centrifugal pump performance characteristics. Int. J. Rotating Mach. 2013.

Logan, Jr, E., 2003. Handbook of turbomachinery. CRC Press.

Mahieddine, M., 1987. Prédetermination des caractéristiques d'une pompe centrifuge, multicellulaire à partir de ses données géométriques. CNAM.

Daily, J.W., Nece, R.E., 1960. Chamber dimension effects on induced flow and frictional resistance of enclosed rotating disks. J. Fluids Eng. 146 (6) https://doi.org/10.1115/1.3662532.

Eça, L., Hoekstra, M., 2014. A procedure for the estimation of the numerical uncertainty of CFD calculations based on grid refinement studies. J. Comput. Phys. 262, 104–130.

Wei, Y., et al., 2023. Numerical investigation of unsteady pressure pulsation characteristics in an ultra-low specific-speed centrifugal pump as a turbine. Front. Energy Res. 10, 1026886.

Lin, T., et al., 2021a. Application of enstrophy dissipation to analyze energy loss in a centrifugal pump as turbine. Renew. Energy 163, 41–55.

Štefan, D., et al., 2020. Study of the internal flow field in a pump-as-turbine (PaT): numerical investigation, overall performance prediction model and velocity vector analysis, 156, 158–172.

Li, J., Meng, D., Qiao, X., 2020. Numerical investigation of flow field and energy loss in a centrifugal pump as turbine. Shock Vib. 2020, 1–12.

Rossi, M., Nigro, A., Renzi, M., 2019. Experimental and numerical assessment of a methodology for performance prediction of Pumps-as-Turbines (PaTs) operating in off-design conditions. Appl. Energy 248, 555–566. https://doi.org/10.1016/j.apenergy.2019.04.123.

Adu, D., et al., 2019. Numerical investigation of transient vortices and turbulent flow behaviour in centrifugal pump operating in reverse mode as turbine, 2 (2), 356–364.

Frosina, E., D. Buono, and A.J.E. Senatore, *A performance prediction method for pumps as turbines (PAT) using a computational fluid dynamics (CFD) modeling approach*. 2017. **10**(1): p. 103.

Bai, X., et al., *Numerical investigation on the blade load distribution in a pump as turbine.* Frontiers in Energy Research. **11**: p. 1220395.

Jianguo, D., et al., *Computational Analysis on Numerical Simulation of Internal flow Physics for Pump as Turbine in Renewable Small Hydro Energy Generation.* 2022. **11**(1): p. 27-36.

Lin, T., et al., 2021b. Theoretical, experimental, and numerical methods to predict the best efficiency point of centrifugal pump as turbine. Renew. Energy 168, 31–44.
Liu, M., Tan, L., Cao, S., 2022. Performance prediction and geometry optimization for application of pump as turbine: a review. Front. Energy Res. 9, 818118.
Liu, M., Tan, L., Cao, S., 2019b. Theoretical model of energy performance prediction and BEP determination for centrifugal pump as turbine. Energy 172, 712–732.